Dye-Sensitized Nonstoichiometric Strontium Titanate Core–Shell Photocathodes for Photoelectrosynthesis Applications

Caroline E. Reilly,[‖] Robert J. Dillon,[‖] Animesh Nayak, Shane Brogan, Taylor Moot, Matthew K. Brennaman, Rene Lopez, Thomas J. Meyer,* and Leila Alibabaei*

ABSTRACT: A core–shell approach that utilizes a high-surface-area conducting core and an outer semiconductor shell is exploited here to prepare p-type dye-sensitized solar energy cells that operate with a minimal applied bias. Photocathodes were prepared by coating thin films of nanocrystalline indium tin oxide with a 0.8 nm Al_2O_3 seeding layer, followed by the chemical growth of nonstoichiometric strontium titanate. Films were annealed and sensitized with either a porphyrin chromophore or a chromophore–catalyst molecular assembly consisting of the porphyrin covalently tethered to the ruthenium complex. The sensitized photoelectrodes produced cathodic photocurrents of up to −315 $\mu A/cm^2$ under simulated sunlight (AM1.5G, 100 mW/cm^2) in aqueous media, pH 5. The photocurrent was increased by the addition of regenerative hole donors to the system, consistent with slow interfacial recombination kinetics, an important property of p-type dye-sensitized electrodes.

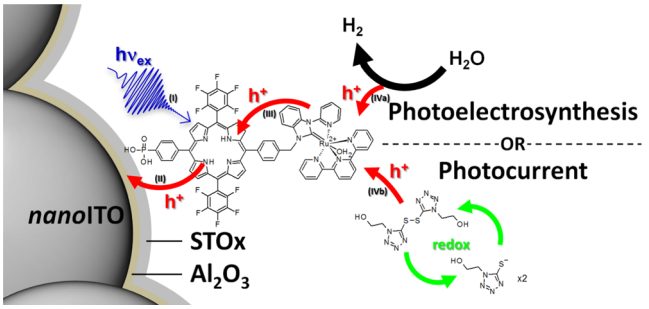

KEYWORDS: *strontium titanate, photocathodes, core–shell, dye-sensitized photoelectrosynthesis cell, hole transfer, artificial photosynthesis*

INTRODUCTION

Dye-sensitized solar cells (DSSCs) and photoelectrosynthesis cells (DSPECs) have progressed considerably in the efficient conversion of solar energy into electrical energy and fuels.[1−5] The ideal DSPEC device employs a tandem design, including a dye-sensitized photoanode and a dye-sensitized photocathode, both utilizing solar energy to drive the two halves of a redox reaction.[6−9] Photoanodes for DSPECs and DSSCs that utilize traditional nanoporous TiO_2, SnO_2, or core–shell SnO_2–TiO_2 metal oxide materials have evolved considerably in this area.[10−16] The development of photocathodes, however, has progressed at a substantially slower rate.[17−19]

Strontium titanate has been touted as a promising material for photoelectrosynthetic applications due to its ability to photo-oxidize water without an externally applied bias.[20,21] Compact $SrTiO_3$ layers have been prepared using a range of deposition methods, including pulsed laser deposition (PLD),[22] spray pyrolysis,[20,23] atomic layer deposition (ALD),[24,25] electrochemical deposition,[26] radio frequency magnetron sputtering,[27,28] and spin-coating.[29,30] Although chemical deposition offers many benefits, such as solution processing, better scale-up possibilities, and less waste, surprisingly few studies have been conducted on the utilization of solution-based methods in the preparation of $SrTiO_3$.[31] Based on our experience, drop-casting of strontium titanate precursors represents a simple but effective method to prepare nonstoichiometric strontium titanate (STOx).

As an added advantage, the solution-based method can also be applied to the construction of core–shell photoelectrodes.[11] In the core–shell approach, a thin, semiconductor shell is applied on a film of conductive transparent nanoparticles, enabling the efficient transport of photogenerated carriers from the shell to the core. The core–shell nanoarchitecture mitigates some of the issues that commonly limit the photocurrent and performance observed in dye-sensitized metal oxide electrodes, e.g., the slow charge transport that facilitates charge recombination at the interface with the dye.[11] This recombination pathway is inhibited by the use of thin shells of the metal oxide material. Poor dye uptake is a known issue for $SrTiO_3$ electrodes when the synthetic method is limited to producing a planar film, including pulsed laser deposition.[21,32] The application of a conformal shell to a mesoporous, high-surface-area core material results in a high-surface-area version of the shell material, which substantially increases dye loading compared to flat films of the same shell material.

Received: January 14, 2021
Accepted: March 2, 2021
Published: March 22, 2021

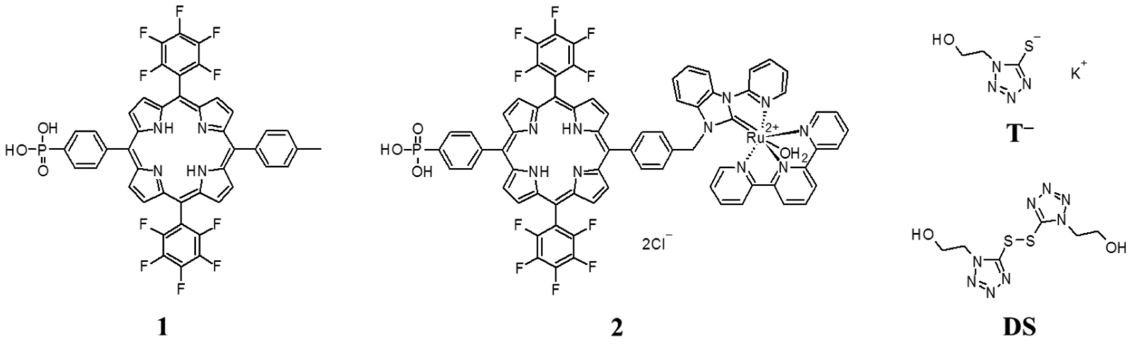

Figure 1. Chemical structures of compound **1**, the porphyrin chromophore, compound **2**, the porphyrin–catalyst assembly, and T^-/**DS**, the thiolate/disulfide redox couple.

Previously, nanocrystalline core–shell thin films of indium tin oxide (*nano*ITO) and TiO_2 have been produced by ALD of conformal films of TiO_2 that encase *nano*ITO particles.[11] In the present study, nonstoichiometric strontium titanate (STOx) shells were chemically grown on *nano*ITO using a simple drop-casting method. With the application of an Al_2O_3 seeding layer to the *nano*ITO before STOx growth, conformal core–shell nanoporous electrodes were fabricated. The resulting *nano*ITO-Al_2O_3-STOx electrodes produced using this method exhibit p-type behavior, suggesting a modified band structure compared to $SrTiO_3$.[33,34]

In this study, two dyes were used to evaluate *nano*ITO-Al_2O_3-STOx electrodes (Figure 1): 5,15-bis-(pentafluorophenyl)-10-(4-methylphenyl)-20-(4-dihydroxyphosphorylphenyl)porphyrin (**1**) and [Ru^{II}(2,2′:6,2″-terpyridine)(1-(2-pyridyl)-3-(5,15-bis-(pentafluorophenyl)-10-(4-methylphenyl)-20-(4-dihydroxyphosphorylphenyl)porphyrin)benzimidazole)-(OH_2)]$^{2+}$ (**2**). The pentafluorophenyl groups on the dye shift their excited-state reduction potential to a more positive value, which facilitates photoinduced hole injection. The phosphonate group provides a superior anchor to the semiconductor surface under aqueous conditions (compared to a carboxylate group).[35] Whereas compound **1** functions solely as a light absorber, compound **2** is a chromophore–catalyst assembly, where a ruthenium-based catalyst is covalently attached to compound **1**. The catalyst moiety of **2** has shown promise in catalytic water-splitting, CO_2 reduction, and syngas applications.[36−38] Here, *nano*ITO-Al_2O_3-STOx electrodes sensitized with compounds **1** and **2** are compared by photocurrent measurements, with and without the added redox couple, 1-(2-hydroxyethyl)-5-mercaptotetrazole (T^-) with its disulfide dimer (**DS**) (Figure 1). Utilizing this porphyrin dye, the aqueous thiolate/disulfide redox shuttle, and the core–shell approach, dye-sensitized *nano*ITO-Al_2O_3-STOx photocathodes demonstrate intramolecular electron transfer with photocurrent responses of up to −315 $\mu A/cm^2$ upon illumination with 1 sun (AM1.5G, 100 mW/cm^2) in aqueous media at pH 5. The photocathodic performance is subsequently discussed in terms of energetics and excited-state redox potentials to infer the properties of the *nano*ITO-Al_2O_3-STOx band structure.

EXPERIMENTAL PROCEDURES

Film Preparation. Mesoporous films of *nano*ITO were prepared using a previously reported method.[11] Fluorine-doped tin oxide (FTO) glass (TEC-15, Hartford glass Co. Inc.) was cut into 2 cm × 4 cm strips and cleaned through sonication in ethanol for two 20 min periods (Branson 2510). A *nano*ITO suspension was prepared by adding 1.5 g of *nano*ITO powder (20 nm particles, Lihochem, Inc.) and 1.42 mL of acetic acid (glacial, Fisher Scientific) to 5.0 mL of ethanol (Decon, 200 proof). The suspension was sonicated for 20 min followed by ultrasonication using a digital sonifier (Branson, model 450, 30% power, 17% duty cycle; 5 min) equipped with an ultrasonic horn outfitted with a flat microtip. Kapton tape was used to cover more than half of each FTO substrate, leaving an exposed area of 2 cm × 1.5 cm. Spin-coating of the *nano*ITO suspension on the substrates was conducted at 600 rpm for 10 s. The films were then annealed in a furnace (Lindberg/Blue M Box Furnace) under air at 500 °C for 1 h, with a 1 h ramp to reach the set annealing temperature to produce light-yellow *nano*ITO films.

A shell-seeding layer of Al_2O_3 (0.8 nm) was deposited through ALD (Cambridge NanoTech, Savannah S200). An exposure-mode treatment at 130 °C was performed with trimethylaluminum as the precursor and nitrogen gas as the flow and purge gas. Five cycles of Al_2O_3 were deposited as follows: 0.02 s precursor pulse, 20 s hold, 60 s N_2 purge, 0.02 s H_2O pulse, 20 s hold, and 60 s N_2 purge. An aluminum oxide film thickness of 0.8 nm was measured using ellipsometry (J.A. Woollam, Variable Angle Spectroscopic Ellipsometer) on flat, silicon wafers that were present in the ALD chamber along with the *nano*ITO films during the ALD process. Nonstoichiometric strontium titanate, STOx, was deposited by drop-casting 150 μL of a solution containing strontium acetate (0.0354 g, Sigma Aldrich), titanium (IV) isopropoxide (0.04 mL, TTIP, Sigma Aldrich), ethyl alcohol (16 mL, Sigma Aldrich), and acetic acid (4 mL, Fisher). The *nano*ITO substrate was placed in a 100 mL jar and, using a Fisherbrand Finnpipette, two runs of 75 μL of solution were slowly dropped onto the substrate for a total volume of 150 μL. The rate of solvent evaporation was regulated by capping the jar with a lid featuring an 11 mm aperture. The films were dried for approximately 18 h. Postdeposition annealing was first performed under atmospheric conditions at 500 °C with a box oven according to a heating program (Table S1), and then at 500 °C in a 2% H_2 atmosphere (98% N_2, Airgas) with a (Lindberg/Blue) tube furnace.

Compound **1** was synthesized using a previously published procedure.[35] The synthesis of compound **2** as a covalently linked assembly of the porphyrin and the catalyst was also based on a previously published procedure.[39] Dye loading of the films was completed by submerging the STOx films in 1 mM porphyrin, mixed-solvent solutions composed of dichloromethane and methanol at a 9:1 (v:v) ratio for 50 min. The dye-loading process was monitored by recording UV–vis absorption measurements at 10 min intervals until the electrodes reached maximum dye loadings (Figure S1).[40] The UV–vis absorption spectra of the dye-sensitized electrodes before and after loading are displayed in Figure S2. The thiolate/disulfide redox shuttle was synthesized according to a previously published procedure.[41] DSSC devices were constructed with *nano*ITO-Al_2O_3-STOx-**1** and Pt-coated FTO electrodes using a previously reported procedure.[42]

Film Characterization. Scanning electron microscopy (SEM) was conducted using a cold-cathode, field-emission scanning electron microscope (Hitachi, S-4700) at an accelerating voltage of 2.0 kV.

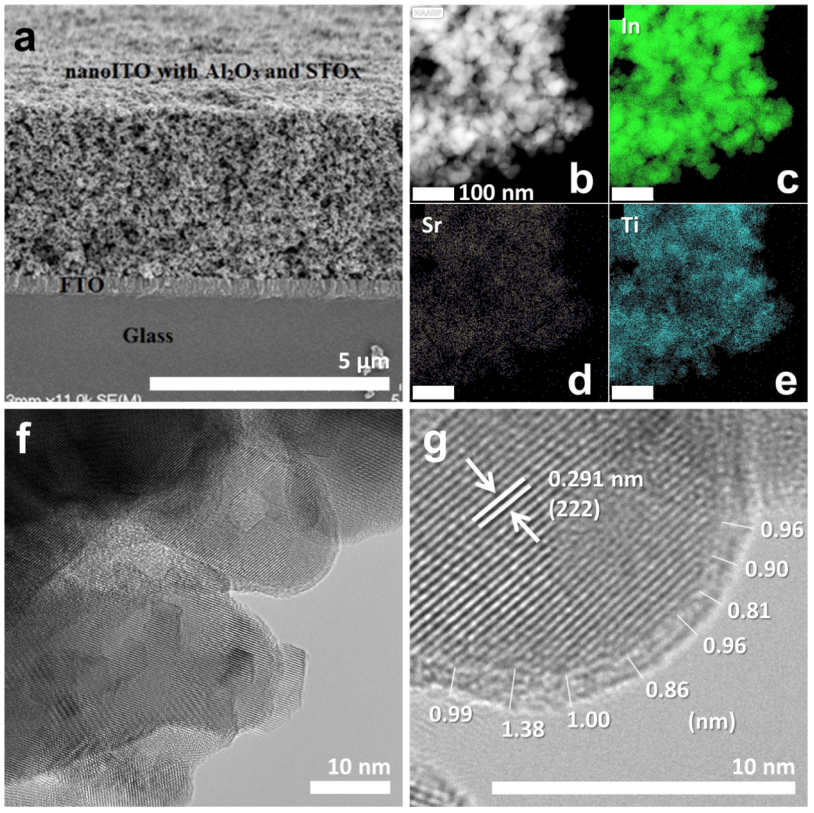

Figure 2. Cross-sectional SEM image of a *nano*ITO-Al_2O_3-STOx film (a), STEM (HAADF) imaging and EDS elemental mapping (b–e), and HRTEM images (f, g) of nanoparticles scraped from a *nano*ITO-Al_2O_3-STOx film. Shell-thickness measurements in (g) were performed with custom LabView software.

Films were sputter-coated (Cressington, 108 auto sputter coater) with 2.0 nm of Au/Pd (60:40 Au:Pd) before SEM imaging. SEM energy dispersive spectroscopy (EDS) was conducted at an accelerating voltage of 20.0 kV using an Oxford Instruments INCA PentaFET-x3 detector. Transmission electron microscopy (TEM) was conducted using a TEM (JEOL, 2010F-FasTEM) and Thermofisher Talos F200X at an accelerating voltage of 200.0 kV. The sample was scraped from the substrate, redispersed in ethanol, and drop-cast on a TEM formvar carbon grid. The imaging was done in both TEM and scanning transmission electron microscopy (STEM) (high-angle annular dark-field, HAADF) modes. Measurements of the shell thickness were done on high-resolution transmission electron microscopy (HRTEM) images with custom image processing software made in LabView. Measurements of the lattice spacing were done via Fourier transform of a region of interest of the HRTEM image, also with custom LabView software. A UV–vis absorption spectrophotometer (Varian, Cary 50) was used to record absorption spectra at a fast scan rate by placing the film or the solution in the path of the beam. Absorption data were collected at 1 nm intervals.

Photoelectrochemistry. Photocurrent–time measurements were performed using *nano*ITO-Al_2O_3-STOx-**1** and *nano*ITO-Al_2O_3-STOx-**2** as working electrodes in a three-electrode configuration. The samples were immersed in aqueous 0.1 M acetate buffer at pH 5 with 1 M $NaClO_4$. A bias of 0 V vs Ag/AgCl was applied using a potentiostat (CH Instruments Inc., 601D) with a Pt-wire counter electrode and an aqueous Ag/AgCl (satd. NaCl, BASi) reference electrode. In addition to the buffer solution, 0.05 M thiolate/disulfide and 1% (v/v) Triton X100 were also added for one series of experiments. For all photocurrent measurements, 1 sun illumination (100 mW/cm^2) was provided by a solar simulator (Newport, 1000 W Xe lamp & AM1.5G filter). Measurements were recorded from the dye-loaded films in a closed cell that had previously been sparged with argon for 10 min.

Steady-State Emission. FTO-ZrO_2-**1** electrodes were placed in an open-topped cuvette (quartz, 1 cm path length). Room-temperature photoluminescence spectra (625–800 nm, 1 nm step size, 0.3 s integration time, 3–5 averages, 90° geometry) were collected using a commercial emission spectrophotometer (PTI, QuantaMaster 4SE-NIR). Photoexcitation at 440 nm was produced by focusing white light from a 75 W Xe lamp into a monochromator (Czerny-Turner, ≤ 4 nm spectral bandwidth). The excitation beam was passed through a 300 nm long-pass filter and then through a beam splitter to direct a portion of the excitation beam onto a Si reference detector to account for fluctuations in the Xe lamp intensity. Emission from the electrodes was passed through a 515 nm long-pass filter, then sent through a monochromator (Czerny-Turner, ≤4 nm spectral bandwidth), and detected with a thermoelectrically cooled (−20 °C) photomultiplier tube (R928P, Hamamatsu Inc.). Emission spectra were corrected for the instrument response and transmission of the 515 nm long-pass filter.

Electrochemistry. A potentiostat (CH Instruments, Inc., 6012D) was used to collect cyclic voltammograms of compound **1** on *nano*ITO in CH_2Cl_2 with 0.1 M $TBAPF_6$ in the open air. The counter electrode consisted of a Pt-wire and the reference electrode was either a Ag wire pseudo-reference electrode or a Ag/$AgNO_3$ (0.1 M $AgNO_3$) reference electrode. The scan rate was 10 mV/s. Potentials recorded relative to a Ag wire reference electrode were converted to the normal hydrogen electrode (NHE) scale by adding +0.682 V to the potentials, with ferrocene serving as an internal standard.[43]

RESULTS AND DISCUSSION

A solution-based method for the chemical deposition of STOx was used to prepare *nano*ITO-Al_2O_3-STOx core–shell photocathodes for DSPEC evaluation. Preparation of the crystalline, stoichiometric form of strontium titanate, $SrTiO_3$, was not possible without damaging the FTO substrate during the

required high-temperature annealing process.[21] Drop-casting was chosen as a relatively low-temperature method for preparing a core−shell electrode with a nonstoichiometric strontium titanate, STOx, shell in the place of stoichiometric $SrTiO_3$. Similar solution-based depositions have been used successfully for related materials, such as lead zirconate titanate.[44,45] Here, prior to drop-casting, an ultrathin (0.8 nm) Al_2O_3 layer was applied onto the *nano*ITO using ALD to serve as a thin seeding shell for growing the STOx layer throughout the *nano*ITO film. The capability of ALD to deposit homogeneous surface coatings on mesoporous metal oxides is well documented.[46,47] Interstitial Al_2O_3 within core−shell electrodes does not interfere with shell-to-core electron transfer for sufficiently thin shells.[48] The use of the controlled evaporation method to apply the STOx precursor solution to the *nano*ITO-Al_2O_3 film was necessary for a deposition without loss of the film by peeling during evaporation. Shown in Figure 2a, the final *nano*ITO-Al_2O_3-STOx film produced after annealing was intact and adhered to the FTO glass substrate, uniform on the micrometer scale, and, most importantly, retains the high surface area of the underlying *nano*ITO film.[49] EDS elemental mapping, Figure 2b−e, shows the presence of Sr and Ti throughout the material, at a ratio of 1:4, Sr:Ti (see Figure S3 and Tables S2 and S3 for full EDS data). HRTEM imaging, Figure 2f,g, reveals highly crystalline core nanoparticles coated with an amorphous shell layer. The lattice spacing corresponds to (222) planes of In_2O_3.[50−52] The sharp distinction between the crystalline core and amorphous shell is utilized to measure the thickness of the latter, which is 1.0 ± 0.2 nm. Given the initial Al_2O_3 layer is 0.8 nm, the STOx layer is an ultrathin ∼0.2 nm.

The shortcomings of solution-based methods to uniformly coat mesoporous materials have been reported previously.[53] While EDS mapping shows Sr and Ti are distributed throughout the material, the uniformity of the STOx layer is inconclusive owing to its extreme thinness, which is within the error of the measurements used to evaluate it. The 1:4 ratio of Sr:Ti calls into question whether some regions of the shell are predominantly composed of TiO_2. However, as shown below, photoanodic currents expected for dye-sensitized TiO_2 are not observed, even for large positive applied potentials.[35] Moreover, the presence of STOx is absolutely critical for the functioning of the photoelectrodes with dye-sensitized samples without STOx exhibiting negligible photocurrents (Figure S4).

Electrodes composed of *nano*ITO-Al_2O_3-STOx-**1** and *nano*ITO-Al_2O_3-STOx-**2** immersed in aqueous pH 5 electrolyte were illuminated with 1 sun (Figure 3a). The photoresponse of *nano*ITO-Al_2O_3-STOx without a dye was negligible ("blank" in Figure 3a), as was for the dye on *nano*ITO or *nano*ITO-Al_2O_3 without STOx (Figure S4). A cathodic photocurrent was observed for *nano*ITO-Al_2O_3-STOx-**1** with a peak photocurrent density of −21 $\mu A/cm^2$ (Figure 3a). The observed photocurrent exceeds the nanoamp photocurrents observed in a previous study on flat $SrTiO_3$ (fabricated via PLD) sensitized with a similar porphyrin dye and is similar to the performance of Ru^{II} polypyridyl dyes on mesoporous NiO.[21,54] The photocathodic response observed for *nano*ITO-Al_2O_3-STOx-**1** is consistent with net, photoinduced hole transfer from the porphyrin ring to the *nano*ITO-Al_2O_3-STOx substrate, as summarized in eq 1a. Photoexcitation of *nano*ITO-Al_2O_3-STOx-**1** generates the porphyrin excited state, Porph*, eq 1a, followed by hole injection from Porph* to the STOx layer to produce STOx(h^+) and $Porph^-$, eq 1b. The ground state is restored via interfacial electron−hole recombination, eq 1c.

$$\text{STOx} - \text{Porph} \xrightarrow{h\nu} \text{STOx} - \text{Porph}^* \quad (1a)$$

$$\text{STOx} - \text{Porph}^* \rightarrow \text{STOx}(h^+) - \text{Porph}^- \quad (1b)$$

$$\text{STOx}(h^+) - \text{Porph}^- \rightarrow \text{STOx} - \text{Porph} \quad (1c)$$

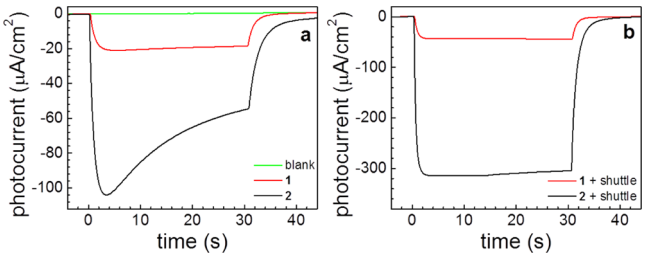

Figure 3. Photocurrent−time traces observed upon 1 sun illumination of *nano*ITO-Al_2O_3-STOx without dye (green) and loaded with compounds **1** (red) and **2** (black) in the absence (a) and presence of the thiolate/disulfide redox shuttle (b). Electrodes were immersed in argon-saturated, 0.1 M acetate buffer, pH 5, in 0.5 M $LiClO_4$. Photoelectrochemical data were collected with E_{bias} = 0 V vs Ag/AgCl.

Incorporation of the dye-catalyst assembly in *nano*ITO-Al_2O_3-STOx-**2** resulted in a photoresponse that decayed over time following a peak photocurrent of −104 $\mu A/cm^2$, a value that is 5 times greater than for the dye alone (Figure 3a). The increase in photocurrent is not attributable to a difference in loading; the loading of **2** is actually slightly less than that of **1**, by a factor of 1.2 (Figure S2). Here, the use of compound **2** in *nano*ITO-Al_2O_3-STOx-**2** was designed to evaluate the chromophore−catalyst assembly as a "push−pull" chromophore as a way to explore its performance without the mechanistic and kinetic constraints of catalysis. Push−pull chromophores with electron-accepting moieties designed to shepherd and shelter excited-state electron density are frequently employed in p-type systems, particularly those based on NiO, and increase device performance by prolonging the lifetime of the charge-separated state.[55,56] Photocathodes of NiO derivatized with dyes without a push−pull design often exhibit interfacial recombination kinetics on the sub-picosecond time scale, which substantially inhibits photoelectrochemical performance.[54,57−60] The increased yet unsustained photocurrent of *nano*ITO-Al_2O_3-STOx-**2** suggests a related but more complex sequence of photoelectrochemical events for the assembly-derivatized electrode compared to the dye-only system, and a kinetically limiting return to the initial state. A hypothetical mechanism is given in eq 2:

$$\text{STOx} - [\text{Porph} - \text{Ru}^{II}]^{2+} \xrightarrow{h\nu} \text{STOx} - [\text{Porph}^* - \text{Ru}^{II}]^{2+} \quad (2a)$$

$$\text{STOx} - [\text{Porph}^* - \text{Ru}^{II}]^{2+} \rightarrow \text{STOx}(h^+) - [\text{Porph}^- - \text{Ru}^{II}]^{+} \quad (2b)$$

$$\text{STOx}(h^+) - [\text{Porph}^- - \text{Ru}^{II}]^{+} \rightarrow \text{STOx}(h^+) - [\text{Porph} - \text{Ru}^{I}]^{+} \quad (2c)$$

As for *nano*ITO-Al_2O_3-STOx-**1**, visible light excitation of *nano*ITO-Al_2O_3-STOx-**2** generates the porphyrin excited-state Porph* (eq 2a), followed by hole injection from Porph* to the STOx layer to produce STOx(h^+) and Porph$^-$ (eq 2b). In *nano*ITO-Al_2O_3-STOx-**2**, the Ru-catalyst moiety of compound **2** serves as a hole donor positioned on the opposite side of the phosphonate anchoring group of the assembly. After hole injection, rapid intra-assembly electron transfer from Porph$^-$ to the Ru^{II} catalyst further separates the electron from the photoinjected hole on the STOx surface and regenerates the porphyrin ground state, Porph (eq 2c). Interfacial charge recombination is presumably inhibited for *nano*ITO-Al_2O_3-STOx(h^+)-[Porph−Ru^I]$^+$ (eq 3) relative to that for *nano*ITO-Al_2O_3-STOx(h^+)-Porph$^-$ due to the increased charge-separation distance as evidenced by the higher photocurrent observed for the assembly-based system.

$$\text{STOx}(h^+) - [\text{Porph} - \text{Ru}^{\text{I}}]^+ \rightarrow \text{STOx} - [\text{Porph} - \text{Ru}^{\text{II}}]^{2+} \quad (3)$$

Diminished interfacial charge recombination results in the slow recovery of compound **2** (eq 3) and is favorable for catalytic applications. From eq 2c, the return of the porphyrin moiety to the neutral ground state primes the system for a second photoinduced hole-injection event in competition with the recovery of the initial state. The faradaic efficiency of the catalyst for water reduction is low, however, decreasing its return to the initial state and is the probable origin for the decrease in photoresponse decays over the course of illumination.[36−38,61]

The photocathodic current for *nano*ITO-Al_2O_3-STOx-**1** doubles to −42 μA/cm^2 upon the addition of thiolate/disulfide (Figure 3b). The simplest explanation for this phenomenon is a rapid reaction of the transiently reduced dye with the redox shuttle to regenerate the ground-state chromophore (eq 4).

$$\text{STOx}(h^+) - \text{Porph}^- + \mathbf{DS} \rightarrow \text{STOx}(h^+) - \text{Porph} + \mathbf{T}^- \quad (4)$$

Similarly, 1 sun illumination of *nano*ITO-Al_2O_3-STOx-**2** with the $\mathbf{T}^-$, **DS** redox shuttle added to the pH 5 electrolyte resulted in a sustained photoresponse over the 30 s illumination interval with a substantial peak photocurrent of −315 μA/cm^2 (Figure 3b). The increase and change in the shape of the photocurrent, from decaying to sustained, for *nano*ITO-Al_2O_3-STOx-**2** in the presence of $\mathbf{T}^-$, **DS** suggest reaction of **DS** with reduced form(s) of the assembly.

An alternative explanation is that the increase in photocurrent upon addition of the redox shuttle is a photogalvanic mechanism in which the photoexcited dye reacts with the preassociated redox electrolyte (eq 5a).[62,63]

$$\text{STOx} - \text{Porph}^* + \mathbf{DS} \rightarrow \text{STOx} - \text{Porph}^+ + \mathbf{T}^- \quad (5a)$$

$$\text{STOx} - \text{Porph}^+ + \mathbf{T}^- \rightarrow \text{STOx}(h^+) - \text{Porph} + \mathbf{T}^- \quad (5b)$$

Nonetheless, a mechanism of this kind appears to be unlikely. The dye exhibits a photocathodic response in the absence of the redox shuttle, which is strong evidence for hole injection in the STOx surface. Moreover, preassociation of the redox shuttle with the dye sensitizer is typically the product of ionic attraction, for example I^-/I_3^- associating with the Ru^{2+} core of a Ru^{II} polypyridyl dye.[64−66] In this study, the relevant form of the redox shuttle, **DS**, is neutral and is not expected to associate with **1** or **2**.

Dye-sensitized solar cell devices were constructed of *nano*ITO-Al_2O_3-STOx-**1**, with Pt-coated FTO electrodes in 0.1 M acetate buffer at pH 5 in 0.5 M $LiClO_4$, using the 0.05 M thiolate/disulfide and 1% (v/v) Triton X100 redox shuttle. The incident photon-to-current efficiency (IPCE) and $J-V$ curves are presented in Figure 4. The shape of the IPCE curve

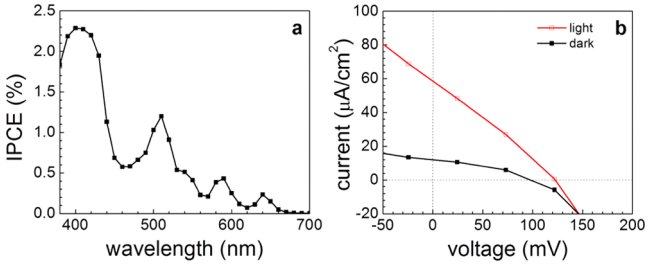

Figure 4. IPCE spectrum (a) and linear sweep voltammetry (b) in the dark and illuminated (1 sun, 100 mW/cm^2) for a DSSC consisting of *nano*ITO-Al_2O_3-STOx-**1** and Pt-coated FTO electrodes, in a 0.1 M acetate buffer at pH 5, in 0.5 M $LiClO_4$, and 0.05 M thiolate/disulfide and 1% (v/v) Triton X100 redox shuttle.

corresponds well with that of the absorption spectrum of the porphyrin, but the efficiency is low, only 2.3% at the Soret band maximum. From the $J-V$ curve, J_{sc} was 59 μA/cm^2, the V_{oc} was 132 mV, the fill factor was 28%, and the efficiency was 0.002%. Despite these lackluster performance characteristics, the results are nevertheless notable in that they are on par with the results reported previously for NiO DSSC electrodes sensitized with porphyrin dyes.[2,67]

In considering cell efficiencies and the photomechanics of hole injection, we focus on the redox potentials and excited-state energetics of compound **1**. From cyclic voltammetry (Figures S5 and S6), the ground-state oxidation, $E^{\circ\prime}(\mathbf{1}^{+/0})$, and reduction potentials, $E^{\circ\prime}(\mathbf{1}^{0/-})$, of compound **1** are 1.78 and −0.22 V vs NHE, respectively. The free energy of the excited state, ΔG_{ES}°, of compound **1** was determined to be 1.95 eV by extrapolating the high-energy side of the corrected emission spectrum (Figure S7) of compound **1** anchored on insulating ZrO_2.[55,56]

$$E^{\circ\prime}(\mathbf{1}^{+/*}) = E^{\circ\prime}(\mathbf{1}^{+/0}) - \Delta G_{ES}^{\circ}/F \quad (6)$$

$$E^{\circ\prime}(\mathbf{1}^{*/-}) = E^{\circ\prime}(\mathbf{1}^{0/-}) - \Delta G_{ES}^{\circ}/F \quad (7)$$

From eqs 6 and 7, where F is the Faraday constant, the excited-state oxidation, $E^{\circ\prime}(\mathbf{1}^{+/*})$, and reduction, $E^{\circ\prime}(\mathbf{1}^{*/-})$, potentials for compound **1** are −0.17 and 1.73 V vs NHE, respectively. The redox potential of the thiolate/disulfide redox couple is 0.325 V vs NHE, according to the literature.[41]

As both the excited-state oxidation and reduction potentials of compound **1** are within the $SrTiO_3$ band gap, photoinduced electron injection and hole injection should not be energetically feasible.[68] Based on these energetics, the observation of a photocurrent from the dye on *nano*ITO-Al_2O_3-STOx is notable. The observation of photocathodic behavior indicates a modified band structure for STOx, one that includes internal redox states that deviate from $SrTiO_3$. One explanation is the presence of intragap states in the nonstoichiometric STOx films. Related studies have observed a potential role for these states in dictating the photophysical processes of dye-sensitized

metal oxide films.[54,69] In $SrTiO_3$-based systems, intragap states have been attributed to various sources, including chemical disorder and electron correlation effects.[70]

Figure 5a shows the photoresponse of *nano*ITO-Al_2O_3-STOx-**1** in argon-saturated, 0.1 M acetate buffer, pH 5, with

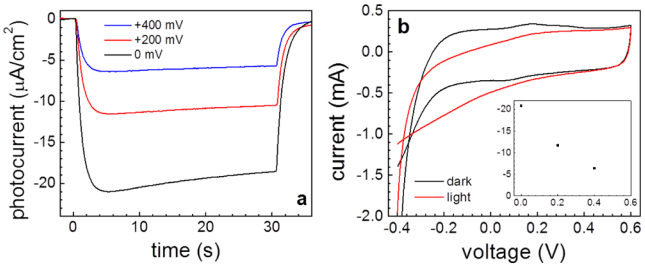

Figure 5. Photocurrent−time traces upon 1 sun illumination of *nano*ITO-Al_2O_3-STOx-**1** for 30 s at increasingly positive applied potentials vs Ag/AgCl (a) and cyclic voltammograms of *nano*ITO-Al_2O_3-STOx-**1** with and without 1 sun illumination (b). The inset in (b) shows the peak photocurrent observed in (a) vs the bias voltage (vs Ag/AgCl). Data in (a) and (b) were collected consecutively on the same electrode immersed in argon-saturated 0.1 M acetate buffer, pH 5, in 0.5 M $LiClO_4$.

0.5 M $LiClO_4$ upon 1 sun illumination as a function of the applied bias. As the bias voltage was increased in small increments, the photocurrent response was significantly diminished. Cyclic voltammetry experiments were conducted under the same conditions with and without 1 sun illumination (Figure 5b) and revealed that the onset of the photoresponse occurred at approximately 0.5 V (vs Ag/AgCl). This value is consistent with what is expected from extrapolating the photocurrent responses in chronoamperometric experiments (Figure 5b, inset). The data of Figure 5 were analyzed to construct a photophysical picture of photoelectrode behavior based on a qualitative understanding of the STOx density of states described in a previous study and the experimental photocurrent response with applied bias.[70] Experimental measurements of the density of states for the STOx films were not conducted.

The proposed mechanism for the photocathodic behavior of compound **1** on STOx with a 0 V (vs Ag/AgCl) applied bias is illustrated in Scheme 1. With the application of the electrochemical bias, a portion of the intragap states is electronically occupied. Following the photoexcitation of the dye, electrons present in the intragap states are energetically able to reduce the photoexcited dye. The reduced dye is then regenerated by the thiolate/disulfide redox shuttle, if present. A band structure in which the intragap states extend downward from the conduction band rather than upwards from the valence band is supported by the disappearance of the photocurrent at applied potentials ≥0.5 V (vs Ag/AgCl). The excited-state reduction potential is much more positive than 0.5 V, and thus hole injection is energetically feasible beyond (more positive than) this potential. The absence of hole injection, however, suggests a lack of intragap states above 0.5 V.

An additional mechanistic consideration for *nano*ITO-Al_2O_3-STOx-**1** is the possibility of competing for photoanodic behavior. Photoexcitation of compound **1** on n-type metal oxides, such as TiO_2 and SnO_2, has been shown to produce photoanodic currents.[39] Electron injection into STOx by the photoexcited dye is thermodynamically feasible because the

Scheme 1. Energy Diagram and Photomechanics of Compound 1 on STOx[a]

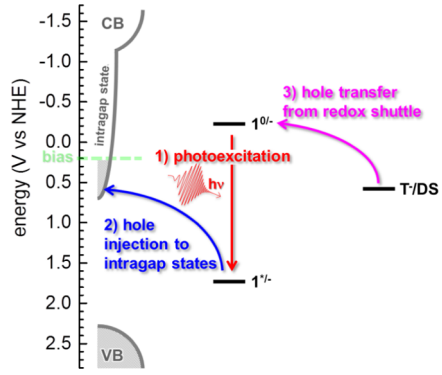

[a]Arrows are drawn illustrating hole transfer. The dashed green line indicates the 0 V (vs Ag/AgCl) applied bias utilized in the photocurrent experiments (+0.206 V vs NHE). The STOx band structure has been qualitatively drawn based on the literature and experimental results obtained in the present study.[70]

excited-state oxidation potential of compound **1** is −0.17 V vs NHE and empty intragap states extend below the conduction band. The observation of overall photocathodic currents for *nano*ITO-Al_2O_3-STOx-**1** suggests that a competing electron injection process must be minimal, if it plays a role. In a similar p-type system, dye-sensitized NiO, electron injection into unoccupied intragap states is not observed, despite favorable thermodynamics.[54]

CONCLUSIONS

Dye-sensitized p-type photoelectrodes that operate with a minimal applied bias by integrating nonstoichiometric strontium titanate, a porphyrin dye, and a dye-catalyst assembly are described here. The high surface area, core−shell *nano*ITO-Al_2O_3-STOx electrodes were prepared with the STOx layer formed by a simple drop-cast solution method. The 1 sun illumination of the dye-sensitized core−shell *nano*ITO-Al_2O_3-STOx results in cathodic photocurrent responses that are 2−3 orders of magnitude higher than those observed for electrodes based on flat $SrTiO_3$, as previously reported.[21] Photocurrents for dye-sensitized *nano*-ITO-Al_2O_3-STOx electrodes are enhanced by the addition of regenerative hole donors, indicating slow interfacial recombination kinetics. These results establish the *nano*ITO-Al_2O_3-STOx-based electrodes presented here as promising candidates for p-type dye-sensitized applications.

ASSOCIATED CONTENT

Supporting Information

The Supporting Information is available free of charge at https://pubs.acs.org/doi/10.1021/acsami.1c00933.

Heating program for postdeposition annealing (Table S1); UV-visible absorption vs. time during dye-loading (Figure S1); UV-visible absorption spectra (Figure S2); EDS elemental mapping (Figure S3); elemental compositions from EDS (Tables S2 and S3); photocurrent−time traces of *nano*ITO-**1** and *nano*ITO-Al_2O_3-**1** (Figure S4); cyclic voltammograms of *nano*ITO-**1** (Figures S5 and S6); emission spectrum of ZrO_2-**1** (Figure S7) (PDF)

AUTHOR INFORMATION

Corresponding Authors

Thomas J. Meyer − *Department of Chemistry, University of North Carolina at Chapel Hill, Chapel Hill, North Carolina 27599, United States;* orcid.org/0000-0002-7006-2608; Email: tjmeyer@unc.edu

Leila Alibabaei − *Department of Chemistry, University of North Carolina at Chapel Hill, Chapel Hill, North Carolina 27599, United States;* orcid.org/0000-0001-5106-0351; Email: alibabaei.leila@gmail.com

Authors

Caroline E. Reilly − *Department of Chemistry, University of North Carolina at Chapel Hill, Chapel Hill, North Carolina 27599, United States*

Robert J. Dillon − *Department of Chemistry, University of North Carolina at Chapel Hill, Chapel Hill, North Carolina 27599, United States;* orcid.org/0000-0002-2248-1306

Animesh Nayak − *Department of Chemistry, University of North Carolina at Chapel Hill, Chapel Hill, North Carolina 27599, United States*

Shane Brogan − *Department of Applied Physical Sciences, University of North Carolina at Chapel Hill, Chapel Hill, North Carolina 27599, United States*

Taylor Moot − *Department of Chemistry, University of North Carolina at Chapel Hill, Chapel Hill, North Carolina 27599, United States;* orcid.org/0000-0002-3528-634X

Matthew K. Brennaman − *Department of Chemistry, University of North Carolina at Chapel Hill, Chapel Hill, North Carolina 27599, United States;* orcid.org/0000-0003-2364-3044

Rene Lopez − *Department of Physics and Astronomy, University of North Carolina at Chapel Hill, Chapel Hill, North Carolina 27599, United States;* orcid.org/0000-0001-6274-066X

Complete contact information is available at: https://pubs.acs.org/10.1021/acsami.1c00933

Author Contributions

[‖]C.E.R. and R.J.D. contributed equally to this work.

Notes

The authors declare no competing financial interest.

ACKNOWLEDGMENTS

This research was solely supported by the Alliance for Molecular Photoelectrode Design for Solar Fuels (AMPED) EFRC, an Energy Frontier Research Center funded by the U.S. Department of Energy, Office of Science, Office of Basic Energy Sciences, under Award No. DE-SC0001011. C.E.R. acknowledges the Office for Undergraduate Research at the University of North Carolina at Chapel Hill for partial funding through an individual Summer Undergraduate Research Fellowship. This study used instrumentation (ALD, ellipsometry, TEM, and SEM) available at the Chapel Hill Analytical and Nanofabrication Laboratory (CHANL), a member of the North Carolina Research Triangle Nanotechnology Network (RTNN), which is supported by the National Science Foundation (Grant ECCS-1542015) as part of the National Nanotechnology Coordinated Infrastructure (NNCI).

REFERENCES

(1) Hamann, T. W.; Jensen, R. A.; Martinson, A. B. F.; Van Ryswyk, H.; Hupp, J. T. Advancing beyond Current Generation Dye-Sensitized Solar Cells. *Energy Environ. Sci.* **2008**, *1*, 66−78.

(2) Nikolaou, V.; Charisiadis, A.; Charalambidis, G.; Coutsolelos, A. G.; Odobel, F. Recent Advances and Insights in Dye-Sensitized NiO Photocathodes for Photovoltaic Devices. *J. Mater. Chem. A* **2017**, *5*, 21077−21113.

(3) Alibabaei, L.; Brennaman, M. K.; Meyer, T. J. Light-Driven Water Splitting in the Dye-Sensitized Photoelectrosynthesis Cell. In *Molecular Devices for Solar Energy Conversion and Storage*; Tian, H.; Boschloo, G.; Hagfeldt, A., Eds.; Springer: Singapore, 2018; pp 229−257. https://doi.org/10.1007/978-981-10-5924-7_6.

(4) Armaroli, N.; Balzani, V. Solar Electricity and Solar Fuels: Status and Perspectives in the Context of the Energy Transition. *Chem. - Eur. J.* **2016**, *22*, 32−57.

(5) Xu, P.; Huang, T.; Huang, J.; Yan, Y.; Mallouk, T. E. Dye-Sensitized Photoelectrochemical Water Oxidation through a Buried Junction. *Proc. Natl. Acad. Sci. U.S.A.* **2018**, *115*, No. 201804728.

(6) Nattestad, A.; Mozer, A. J.; Fischer, M. K. R.; Cheng, Y.-B.; Mishra, A.; Bäuerle, P.; Bach, U. Highly Efficient Photocathodes for Dye-Sensitized Tandem Solar Cells. *Nat. Mater.* **2010**, *9*, 31−35.

(7) Li, F.; Fan, K.; Xu, B.; Gabrielsson, E.; Daniel, Q.; Li, L.; Sun, L. Organic Dye-Sensitized Tandem Photoelectrochemical Cell for Light Driven Total Water Splitting. *J. Am. Chem. Soc.* **2015**, *137*, 9153−9159.

(8) Sherman, B. D.; Sheridan, M. V.; Wee, K. R.; Marquard, S. L.; Wang, D.; Alibabaei, L.; Ashford, D. L.; Meyer, T. J. A Dye-Sensitized Photoelectrochemical Tandem Cell for Light Driven Hydrogen Production from Water. *J. Am. Chem. Soc.* **2016**, *138*, 16745−16753.

(9) Benazzi, E.; Mallows, J.; Summers, G. H.; Black, F. A.; Gibson, E. A. Developing Photocathode Materials for p-Type Dye-Sensitized Solar Cells. *J. Mater. Chem. C* **2019**, *7*, 10409−10445.

(10) Alibabaei, L.; Brennaman, M. K.; Norris, M. R.; Kalanyan, B.; Song, W.; Losego, M. D.; Concepcion, J. J.; Binstead, R. A.; Parsons, G. N.; Meyer, T. J. Solar Water Splitting in a Molecular Photoelectrochemical Cell. *Proc. Natl. Acad. Sci. U.S.A.* **2013**, *110*, 20008−20013.

(11) Alibabaei, L.; Farnum, B. H.; Kalanyan, B.; Brennaman, M. K.; Losego, M. D.; Parsons, G. N.; Meyer, T. J. Atomic Layer Deposition of TiO2 on Mesoporous NanoITO: Conductive Core-Shell Photoanodes for Dye-Sensitized Solar Cells. *Nano Lett.* **2014**, *14*, 3255−3261.

(12) Leem, G.; Sherman, B. D.; Burnett, A. J.; Morseth, Z. A.; Wee, K.-R.; Papanikolas, J. M.; Meyer, T. J.; Schanze, K. S. Light-Driven Water Oxidation Using Polyelectrolyte Layer-by-Layer Chromophore−Catalyst Assemblies. *ACS Energy Lett.* **2016**, *1*, 339−343.

(13) Ganapathy, V.; Karunagaran, B.; Rhee, S.-W. Improved Performance of Dye-Sensitized Solar Cells with TiO2/Alumina Core−Shell Formation Using Atomic Layer Deposition. *J. Power Sources* **2010**, *195*, 5138−5143.

(14) Alibabaei, L.; Sherman, B. D.; Norris, M. R.; Brennaman, M. K.; Meyer, T. J. Visible Photoelectrochemical Water Splitting into H2 and O2 in a Dye-Sensitized Photoelectrosynthesis Cell. *Proc. Natl. Acad. Sci. U.S.A.* **2015**, *112*, 5899−5902.

(15) Alibabaei, L.; Dillon, R. J.; Reilly, C. E.; Brennaman, M. K.; Wee, K. R.; Marquard, S. L.; Papanikolas, J. M.; Meyer, T. J. Chromophore-Catalyst Assembly for Water Oxidation Prepared by Atomic Layer Deposition. *ACS Appl. Mater. Interfaces* **2017**, *9*, 39018−39026.

(16) Brennaman, M. K.; Dillon, R. J.; Alibabaei, L.; Gish, M. K.; Dares, C. J.; Ashford, D. L.; House, R. L.; Meyer, G. J.; Papanikolas, J. M.; Meyer, T. J. Finding the Way to Solar Fuels with Dye-Sensitized Photoelectrosynthesis Cells. *J. Am. Chem. Soc.* **2016**, *138*, 13085−13102.

(17) Odobel, F.; Pellegrin, Y. Recent Advances in the Sensitization of Wide-Band-Gap Nanostructured p-Type Semiconductors. Photovoltaic and Photocatalytic Applications. *J. Phys. Chem. Lett.* **2013**, *4*, 2551−2564.

(18) Odobel, F.; Le Pleux, L.; Pellegrin, Y.; Blart, E. New Photovoltaic Devices Based on the Sensitization of p-Type Semiconductors: Challenges and Opportunities. *Acc. Chem. Res.* **2010**, *43*, 1063−1071.
(19) Wood, C. J.; Summers, G. H.; Clark, C. A.; Kaeffer, N.; Braeutigam, M.; Carbone, L. R.; D'Amario, L.; Fan, K.; Farré, Y.; Narbey, S.; Oswald, F.; Stevens, L. A.; Parmenter, C. D. J.; Fay, M. W.; La Torre, A.; Snape, C. E.; Dietzek, B.; Dini, D.; Hammarström, L.; Pellegrin, Y.; Odobel, F.; Sun, L.; Artero, V.; Gibson, E. A. A Comprehensive Comparison of Dye-Sensitized NiO Photocathodes for Solar Energy Conversion. *Phys. Chem. Chem. Phys.* **2016**, *18*, 10727−10738.
(20) Shih, S.-J.; Widagdyo, D. R. Preparation of Mesoporous SrTiO 3 Particles by Spray Pyrolysis Method. *J. Nanosci. Nanotechnol.* **2017**, *17*, 3557−3565.
(21) Call, R. W.; Alibabaei, L.; Dillon, R. J.; Knauf, R. R.; Nayak, A.; Dempsey, J. L.; Papanikolas, J. M.; Lopez, R. Growth and Post-Deposition Treatments of SrTiO3 Films for Dye-Sensitized Photoelectrosynthesis Cell Applications. *ACS Appl. Mater. Interfaces* **2016**, *8*, 12282−12290.
(22) Call, R. W.; Brogan, S.; Alibabaei, L.; Lopez, R. Impedance Spectroscopy Study of SrTiO3 Pulse Laser Deposited Photoelectrodes. *Thin Solid Films* **2018**, *655*, 27−33.
(23) Branković, G.; Branković, Z.; Varela, J. A.; Longo, E. Strontium Titanate Films Prepared by Spray Pyrolysis. *J. Eur. Ceram. Soc.* **2004**, *24*, 989−991.
(24) Lee, S. W.; Han, J. H.; Han, S.; Lee, W.; Jang, J. H.; Seo, M.; Kim, S. K.; Dussarrat, C.; Gatineau, J.; Min, Y.-S.; Hwang, C. S. Atomic Layer Deposition of SrTiO 3 Thin Films with Highly Enhanced Growth Rate for Ultrahigh Density Capacitors. *Chem. Mater.* **2011**, *23*, 2227−2236.
(25) Suchanek, W. L.; Yoshimura, M. Preparation of Strontium Titanate Thin Films by the Hydrothermal-Electrochemical Method in a Solution Flow System. *J. Am. Ceram. Soc.* **2005**, *81*, 2864−2868.
(26) Suchanek, W. L.; Yoshimura, M. Preparation of Strontium Titanate Thin Films by the Hydrothermal-Electrochemical Method in a Solution Flow System. *J. Am. Ceram. Soc.* **2005**, *81*, 2864−2868.
(27) Nam, S. H.; Kim, H. G. Electrical Properties of the SrTiO3 Thin Films Prepared by Radio Frequency Magnetron Sputtering. *Ferroelectrics* **1994**, *152*, 79−84.
(28) Wang, Z.; Kugler, V.; Helmersson, U.; Evangelou, E. K.; Konofaos, N.; Nakao, S.; Jin, P. Characteristics of SrTiO3 Thin Films Deposited on Si by Rf Magnetron Sputtering at Various Substrate Temperatures. *Philos. Mag. B* **2002**, *82*, 891−903.
(29) Dayalan, E.; Tomar, M. S. Low Temperature Preparation of SrTiO3 Thin Films. *Thin Solid Films* **1993**, *236*, 37−39.
(30) Selvaraj, U.; Prasadarao, A. V.; Komarneni, S.; Roy, R. Sol-Gel Processing of Oriented SrTiO3 Thin Films. *Mater. Lett.* **1995**, *23*, 123−127.
(31) Leite, E. R.; Mastelaro, V. R.; Zanetti, S. M.; Longo, E. Crystallization Study of SrTiO3 Thin Films Prepared by Dip Coating. *Mater. Res.* **1999**, *2*, 93−97.
(32) Burnside, S.; Moser, J.-E.; Brooks, K.; Grätzel, M.; Cahen, D. Nanocrystalline Mesoporous Strontium Titanate as Photoelectrode Material for Photosensitized Solar Devices: Increasing Photovoltage through Flatband Potential Engineering. *J. Phys. Chem. B* **1999**, *103*, 9328−9332.
(33) Moot, T.; Isayev, O.; Call, R. W.; McCullough, S. M.; Zemaitis, M.; Lopez, R.; Cahoon, J. F.; Tropsha, A. Material Informatics Driven Design and Experimental Validation of Lead Titanate as an Aqueous Solar Photocathode. *Mater. Discovery* **2016**, *6*, 9−16.
(34) Chen, F.; Schafranek, R.; Li, S.; Wu, W. B.; Klein, A. Energy Band Alignment between Pb(Zr,Ti)O3and High and Low Work Function Conducting Oxides—from Hole to Electron Injection. *J. Phys. D: Appl. Phys.* **2010**, *43*, No. 295301.
(35) Nayak, A.; Roy, S.; Sherman, B. D.; Alibabaei, L.; Lapides, A. M.; Brennaman, M. K.; Wee, K.-R.; Meyer, T. J. Phosphonate-Derivatized Porphyrins for Photoelectrochemical Applications. *ACS Appl. Mater. Interfaces* **2016**, *8*, 3853−3860.
(36) Chen, Z.; Concepcion, J. J.; Brennaman, M. K.; Kang, P.; Norris, M. R.; Hoertz, P. G.; Meyer, T. J. Splitting CO2 into CO and O2 by a Single Catalyst. *Proc. Natl. Acad. Sci. U.S.A.* **2012**, *109*, 15606−15611.
(37) Kang, P.; Chen, Z.; Nayak, A.; Zhang, S.; Meyer, T. J. Single Catalyst Electrocatalytic Reduction of CO2 in Water to H2+CO Syngas Mixtures with Water Oxidation to O2. *Energy Environ. Sci.* **2014**, *7*, 4007−4012.
(38) Gonell, S.; Assaf, E. A.; Duffee, K. D.; Schauer, C. K.; Miller, A. J. M. Kinetics of the Trans Effect in Ruthenium Complexes Provide Insight into the Factors That Control Activity and Stability in CO2 Electroreduction. *J. Am. Chem. Soc.* **2020**, *142*, 8980−8999.
(39) Nayak, A.; Hu, K.; Roy, S.; Brennaman, M. K.; Shan, B.; Meyer, G. J.; Meyer, T. J. Synthesis and Photophysical Properties of a Covalently Linked Porphyrin Chromophore−Ru(II) Water Oxidation Catalyst Assembly on SnO 2 Electrodes. *J. Phys. Chem. C* **2018**, *122*, 13455−13461.
(40) Pasternack, R. F.; Huber, P. R.; Boyd, P.; Engasser, G.; Francesconi, L.; Gibbs, E.; Fasella, P.; Cerio Venturo, G.; Hinds, L. D. Aggregation of Meso-Substituted Water-Soluble Porphyrins. *J. Am. Chem. Soc.* **1972**, *94*, 4511−4517.
(41) Fayad, R.; Shoker, T. A.; Ghaddar, T. H. High Photo-Currents with a Zwitterionic Thiocyanate-Free Dye in Aqueous-Based Dye Sensitized Solar Cells. *Dalton Trans.* **2016**, *45*, 5622−5628.
(42) Ito, S.; Murakami, T. N.; Comte, P.; Liska, P.; Grätzel, C.; Nazeeruddin, M. K.; Grätzel, M. Fabrication of Thin Film Dye Sensitized Solar Cells with Solar to Electric Power Conversion Efficiency over 10%. *Thin Solid Films* **2008**, *516*, 4613−4619.
(43) Tsierkezos, N. G. Cyclic Voltammetric Studies of Ferrocene in Nonaqueous Solvents in the Temperature Range from 248.15 to 298.15 K. *J. Solution Chem.* **2007**, *36*, 289−302.
(44) Varghese, J.; Ghoshal, T.; Deepak, N.; O'Regan, C.; Whatmore, R. W.; Morris, M. A.; Holmes, J. D. Fabrication of Arrays of Lead Zirconate Titanate (PZT) Nanodots via Block Copolymer Self-Assembly. *Chem. Mater.* **2013**, *25*, 1458−1463.
(45) Reitz, C.; Leufke, P. M.; Hahn, H.; Brezesinski, T. Ordered Mesoporous Thin Film Ferroelectrics of Biaxially Textured Lead Zirconate Titanate (PZT) by Chemical Solution Deposition. *Chem. Mater.* **2014**, *26*, 2195−2202.
(46) Parsons, G. N.; George, S. M.; Knez, M. Progress and Future Directions for Atomic Layer Deposition and ALD-Based Chemistry. *MRS Bull.* **2011**, *36*, 865−871.
(47) Peng, Q.; Lewis, J. S.; Hoertz, P. G.; Glass, J. T.; Parsons, G. N. Atomic Layer Deposition for Electrochemical Energy Generation and Storage Systems. *J. Vac. Sci. Technol., A* **2012**, *30*, No. 010803.
(48) Wang, D.; Farnum, B. H.; Sheridan, M. V.; Marquard, S. L.; Sherman, B. D.; Meyer, T. J. Inner Layer Control of Performance in a Dye-Sensitized Photoelectrosynthesis Cell. *ACS Appl. Mater. Interfaces* **2017**, *9*, 33533−33538.
(49) Chen, Z.; Concepcion, J. J.; Hull, J. F.; Hoertz, P. G.; Meyer, T. J. Catalytic Water Oxidation on Derivatized NanoITO. *Dalton Trans.* **2010**, *39*, 6950−6952.
(50) Ma, K.; Zhou, N.; Yuan, M.; Li, D.; Yang, D. Tunable Surface Plasmon Resonance Frequencies of Monodisperse Indium Tin Oxide Nanoparticles by Controlling Composition, Size, and Morphology. *Nanoscale Res. Lett* **2014**, *9*, No. 547.
(51) Thirumoorthi, M.; Thomas Joseph Prakash, J. Structure, Optical and Electrical Properties of Indium Tin Oxide Ultra Thin Films Prepared by Jet Nebulizer Spray Pyrolysis Technique. *J. Asian Ceram. Soc.* **2016**, *4*, 124−132.
(52) Lacroix, B.; Santos, A. J.; Hurand, S.; Corvisier, A.; Paumier, F.; Girardeau, T.; Maudet, F.; Dupeyrat, C.; García, R.; Morales, F. M. Nanostructure and Physical Properties Control of Indium Tin Oxide Films Prepared at Room Temperature through Ion Beam Sputtering Deposition at Oblique Angles. *J. Phys. Chem. C* **2019**, *123*, 14036−14046.
(53) Lee, S.-H. A.; Zhao, Y.; Hernandez-Pagan, E. A.; Blasdel, L.; Youngblood, W. J.; Mallouk, T. E. Electron Transfer Kinetics in Water

Splitting Dye-Sensitized Solar Cells Based on Core−Shell Oxide Electrodes. *Faraday Discuss.* **2012**, *155*, 165−176.
(54) Dillon, R. J.; Alibabaei, L.; Meyer, T. J.; Papanikolas, J. M. Enabling Efficient Creation of Long-Lived Charge-Separation on Dye-Sensitized NiO Photocathodes. *ACS Appl Mater Interfaces* **2017**, *9*, 26786−26796.
(55) Alstrum-Acevedo, J. H.; Brennaman, M. K.; Meyer, T. J. Chemical Approaches to Artificial Photosynthesis. 2. *Inorg. Chem.* **2005**, *44*, 6802−6827.
(56) Ito, A.; Meyer, T. J. The Golden Rule. Application for Fun and Profit in Electron Transfer, Energy Transfer, and Excited-State Decay. *Phys. Chem. Chem. Phys.* **2012**, *14*, 13731−13745.
(57) Morandeira, A.; Boschloo, G.; Hagfeldt, A.; Hammarström, L. Photoinduced Ultrafast Dynamics of Coumarin 343 Sensitized p-Type-Nanostructured NiO Films. *J. Phys. Chem. B* **2005**, *109*, 19403−19410.
(58) Huang, Z.; Natu, G.; Ji, Z.; He, M.; Yu, M.; Wu, Y. Probing the Low Fill Factor of NiO p-Type Dye-Sensitized Solar Cells. *J. Phys. Chem. C* **2012**, *116*, 26239−26246.
(59) Ji, Z.; Natu, G.; Huang, Z.; Kokhan, O.; Zhang, X.; Wu, Y. Synthesis, Photophysics, and Photovoltaic Studies of Ruthenium Cyclometalated Complexes as Sensitizers for p-Type NiO Dye-Sensitized Solar Cells. *J. Phys. Chem. C* **2012**, *116*, 16854−16863.
(60) Han, Y.; Dillon, R. J.; Flynn, C. J.; Rountree, E. S.; Alibabaei, L.; Cahoon, J. F.; Papanikolas, J. M.; Dempsey, J. L. Interfacial Electron Transfer Yields in Dye-Sensitized NiO Photocathodes Correlated to Excited-State Dipole Orientation of Ruthenium Chromophores. *Can. J. Chem.* **2018**, *96*, 865−874.
(61) Gonell, S.; Massey, M. D.; Moseley, I. P.; Schauer, C. K.; Muckerman, J. T.; Miller, A. J. M. The Trans Effect in Electrocatalytic CO2 Reduction: Mechanistic Studies of Asymmetric Ruthenium Pyridyl-Carbene Catalysts. *J. Am. Chem. Soc.* **2019**, *141*, 6658−6671.
(62) Morandeira, A.; Boschloo, G.; Hagfeldt, A.; Hammarström, L. Coumarin 343-NiO Films as Nanostructured Photocathodes in Dye-Sensitized Solar Cells: Ultrafast Electron Transfer, Effect of the I^{3-}/I^{-} Redox Couple and Mechanism of Photocurrent Generation. *J. Phys. Chem. C* **2008**, *112*, 9530−9537.
(63) Odobel, F.; Pellegrin, Y.; Gibson, E. A.; Hagfeldt, A.; Smeigh, A. L.; Hammarström, L. Recent Advances and Future Directions to Optimize the Performances of p-Type Dye-Sensitized Solar Cells. *Coord. Chem. Rev.* **2012**, *256*, 2414−2423.
(64) Antila, L. J.; Myllyperkiö, P.; Mustalahti, S.; Lehtivuori, H.; Korppi-Tommola, J. Injection and Ultrafast Regeneration in Dye-Sensitized Solar Cells. *J. Phys. Chem. C* **2014**, *118*, 7772−7780.
(65) Swords, W. B.; Li, G.; Meyer, G. J. Iodide Ion Pairing with Highly Charged Ruthenium Polypyridyl Cations in CH3CN. *Inorg. Chem.* **2015**, *54*, 4512−4519.
(66) Casarin, L.; Swords, W. B.; Caramori, S.; Bignozzi, C. A.; Meyer, G. J. Rapid Static Sensitizer Regeneration Enabled by Ion Pairing. *Inorg. Chem.* **2017**, *56*, 7324−7327.
(67) Borgström, M.; Blart, E.; Boschloo, G.; Mukhtar, E.; Hagfeldt, A.; Hammarström, L.; Odobel, F. Sensitized Hole Injection of Phosphorus Porphyrin into NiO: Toward New Photovoltaic Devices. *J. Phys. Chem. B* **2005**, *109*, 22928−22934.
(68) Xu, Y.; Schoonen, M. A. A. The Absolute Energy Positions of Conduction and Valence Bands of Selected Semiconducting Minerals. *Am. Mineral.* **2000**, *85*, 543−556.
(69) Haque, S. A.; Tachibana, Y.; Willis, R. L.; Moser, J. E.; Grätzel, M.; Klug, D. R.; Durrant, J. R. Parameters Influencing Charge Recombination Kinetics in Dye-Sensitized Nanocrystalline Titanium Dioxide Films. *J. Phys. Chem. B* **2000**, *104*, 538−547.
(70) Ishida, Y.; Eguchi, R.; Matsunami, M.; Horiba, K.; Taguchi, M.; Chainani, A.; Senba, Y.; Ohashi, H.; Ohta, H.; Shin, S. Coherent and Incoherent Excitations of Electron-Doped SrTiO 3. *Phys. Rev. Lett.* **2008**, *100*, No. 056401.

NOTE ADDED AFTER ASAP PUBLICATION

Published ASAP on March 22, 2021; Equations 4 and 5a revised March 23, 2021.